Journal of Materials Chemistry A

COMMUNICATION

A dual ternary system for highly efficient ITO-free inverted polymer solar cells†

Zuosheng Peng,[a] Yuxin Xia,[ab] Feng Gao,[bc] Kang Xiong,[a] Zhanhao Hu,[c] David Ian James,[d] Junwu Chen,*[c] Ergang Wang*[d] and Lintao Hou*[a]

Cite this: *J. Mater. Chem. A*, 2015, **3**, 18365

Received 27th May 2015
Accepted 21st July 2015

DOI: 10.1039/c5ta03831f

www.rsc.org/MaterialsA

In this study, it has been found that a very fine nanostructure can be realized by mixing 1-chloronaphthalene (CN) – a high-boiling solvent – into a binary chlorobenzene (CB) : 1,8-diiodooctane (DIO) solvent mixture to form a ternary solvent system. An improvement in energy level alignment is also obtained by doping ICBA into a binary PTB7 : PCBM[70] blend, whereby the ternary solute system provides a new pathway for charge transfer from PTB7 to the PCBM[70] : ICBA alloy. This is confirmed by imaging the surface morphology of the active layer using AFM and TEM, monitoring the transient film formation process and measuring the charge transfer states with Fourier transform photocurrent spectroscopy. An encouraging PCE of 7.65% is achieved from the dual ternary system, which is the highest value ever reported for an ITO-free inverted polymer solar cell with a PEDOT:PSS layer as the top semitransparent electrode – a system which is compatible with low-cost large-area roll-to-roll manufacturing.

Introduction

Solution-processed bulk heterojunction (BHJ) polymer solar cells (PSCs) based on polymer : fullerene blends are now getting closer to commercialization, with the highest power conversion efficiencies (PCEs) now over 10% at the laboratory scale.[1–3] Roll-to-roll coating technologies enable PSCs to be produced on a large scale at low cost compared to batch processed inorganic solar cells.[4,5] To further reduce the cost of PSCs the use of indium tin oxide (ITO), which is extensively used as the transparent electrode in PSCs, should be avoided. Moreover, in conventional device structures, the use of an ITO/poly(3,4-ethylenedioxythiophene):poly(styrenesulfonate) (PEDOT:PSS) stack as the anode and a low work function metal as the cathode reduces the stability of PSCs due to corrosion of the ITO by the acidic PEDOT:PSS layer and oxidation of the low work function metal by air.[6,7] ITO-free inverted solar cells (IFISCs) show greater stability as they employ PEDOT:PSS as the top transparent anode and a bottom metal contact as the cathode making them more compatible with roll-to-roll processing.[8,9]

Previous studies have shown that the morphology of donor : acceptor (D : A) blends greatly affects device performance in addition to the intrinsic properties of the materials that make up the active layer.[10,11] Several treatments to modify blend morphologies have been investigated such as thermal annealing,[12] solvent soaking,[13] various processing methods[14] and a variety of processing solvents to name but a few, in which varying the composition of the solvent mixture is considered to be the most effective approach.[15] 1,8-Diiodooctane (DIO) and 1-chloronaphthalene (CN) have been widely used as additives in organic solvents such as chlorobenzene (CB) or 1,2-dichlorobenzene (DCB) and chloroform (CF),[3,16] to give binary solvent systems.[17,18] Furthermore, a ternary solvent system DCB : CF : DIO has been successfully used to further improve the morphology of BHJ blend films.[19] Compared with widely used binary solvent systems, ternary solvent systems have been rarely studied. Reports of ternary blend BHJ solar cells based on two donors with complementary absorption spectra and one acceptor (D1 : D2 : A) have shown that improved PCEs can be obtained as they show broad absorption, enhanced carrier mobilities and optimal energy levels between the donors and the acceptor.[20–26] Compared to the D1 : D2 : A ternary system, one donor and two acceptor (D : A1 : A2) ternary systems have attracted much less attention as these systems normally cannot extend the absorption spectra of their active layers.[27–29]

In light of lack of a systematic study on the combination of a ternary solvent system with a D : A1 : A2 ternary blend system, which we refer to as a dual ternary system, as well as

[a]Siyun Laboratory, Department of Physics, Jinan University, Guangzhou 510632, P. R. China. E-mail: thlt@jnu.edu.cn

[b]Biomolecular and Organic Electronics, IFM, and Center of Organic Electronics, Linköping University, SE-581 83 Linköping, Sweden

[c]Institute of Polymer Optoelectronic Materials and Devices, State Key Laboratory of Luminescent Materials and Devices, South China University of Technology, Guangzhou 510640, P. R. China. E-mail: psjwchen@scut.edu.cn

[d]Department of Chemistry and Chemical Engineering/Polymer Technology, Chalmers University of Technology, SE-412 96 Göteborg, Sweden. E-mail: ergang@chalmers.se

† Electronic supplementary information (ESI) available. See DOI: 10.1039/c5ta03831f

ITO-free device structures that are more stable, in this study, we employ CB : DIO : CN as the ternary solvent system to investigate D : A1 : A2 ternary blends in ITO-free devices. The low-bandgap polymer thieno[3,4-*b*]thiophene/benzodithiophene (PTB7) is used as the donor and [6,6]-phenyl-C71-butyric acid methyl ester (PCBM[70]) and indene-C60 bisadduct (ICBA) are used as the acceptors in an ITO-free inverted device architecture of glass/Al/TiO_x/active layer/PEDOT:PSS. For extracting electrons from the active layer, a thin layer of poly[(9,9-bis(3′-(*N*,*N*-dimethylamino)propyl)-2,7-fluorene)-*alt*-2,7-(9,9-dioctylfluorene)] (PFN) was incorporated into the IFISC to modify the Al/TiO_x cathode. In order to compare the dual ternary system with a binary solvent system and a normal D : A binary blend system as well as device architectures which use ITO as the electrode, seven different types of solar cell devices were fabricated:

Type 1: glass/Al/TiO_x/PTB7 : PCBM[70] (with a CB : DIO binary solvent system)/PEDOT:PSS.

Type 2: glass/Al/TiO_x/PFN/active layer/PEDOT:PSS.

Active layer:

Type 2a: PTB7 : PCBM[70] with a CB : DIO binary solvent system.

Type 2b: PTB7 : PCBM[70] with a CB : DIO : CN ternary solvent system.

Type 2c: PTB7 : PCBM[70] : ICBA with a CB : DIO : CN ternary solvent system.

Type 3: glass/ITO/PFN/active layer/MoO_3/Al.

Active layer:

Type 3a: PTB7 : PCBM[70] with a CB : DIO binary solvent system.

Type 3b: PTB7 : PCBM[70] with a CB : DIO : CN ternary solvent system.

Type 3c: PTB7 : PCBM[70] : ICBA with a CB : DIO : CN ternary solvent system.

Recently, Chen *et al.* reported ITO-free PSCs with a PEDOT:PSS:carbon nanotube electrode showing a PCE of 7.4%.[30] Tang *et al.* achieved a PCE of 6.70% by incorporating a conjugated polymer poly(3,3′-([(9′,9′-dioctyl-9*H*,9′*H*-[2,2′-bifluorene]-9,9-diyl)bis(4,1-phenylene)]bis(oxy))bis(*N*,*N*-dimethylpropan-1-amine)) as the interlayer with the device structure of substrate/cathode/active layer/PEDOT:PSS.[31] In this study, we decided to use a device structure glass/Al/TiO_x/active layer/PEDOT:PSS with PFN incorporated to modify the Al/TiO_x cathode.[32,33] An average PCE of 6.08% for an IFISC was achieved in Type 2a devices with PTB7 : PCBM[70] as the active layer and CB : DIO as the binary solvent. The active layer film was improved by using the ternary solvent system CB : DIO : CN which yielded an average device efficiency of 6.61% in Type 2b devices. Furthermore, when ICBA was blended into PTB7 : PCBM[70] in the CB : DIO : CN ternary solvent to form a dual ternary system, the average PCE further improved to 7.55% in Type 2c devices. In Type 3 devices which use ITO as the electrode, an improvement in the PCE was also found. Thus, in this study the use of the dual ternary system has been shown to be a viable strategy to improve the efficiency of BHJ solar cells.

Results and discussion

The schematic device structure of the IFISC, the chemical structures of PTB7, PFN, PCBM[70] and ICBA, and the schematic energy levels of various materials are shown in Fig. 1. The active layer is sandwiched between the reflective cathode Al/TiO_x and the transparent anode PEDOT:PSS. Fig. 2a presents the current density *versus* voltage (*J*–*V*) characteristics of IFISCs under AM 1.5G illumination. The detailed parameters of the devices including the short-circuit current density (J_{sc}), open-circuit voltage (V_{oc}), fill factor (FF) and PCE deduced from the *J*–*V* measurements are summarized in Table 1. The Type 1 devices employing the binary solvent system CB : DIO (97 : 3 v/v) without using PFN as the interlayer exhibit an average PCE of 4.13%, which is much lower than the average PCE of 6.08% attained from the Type 2a devices using PFN as the interlayer. When CN was used as the third ingredient to form a ternary solvent system (CB : DIO : CN 94 : 3 : 3 v/v), a higher PCE of 6.61% was achieved for the Type 2b devices. Here we emphasize that 3% CN is the optimal volume ratio for doping the binary solvent system CB : DIO for the PTB7 : PCBM[70] devices in comparison with other doping ratios (1% and 5%), as shown in Fig. S1 and Table S1.† We emphasize that the CB : CN (97 : 3 v/v) binary solvent system shows a lower PCE than the CB : DIO (97 : 3 v/v) binary solvent system (5.72% *vs.* 6.01%). Furthermore, PTB7 : PCBM[70] was doped with different weight ratios (5, 10 and 15 wt%) of ICBA to form a ternary solute system in conjunction with the ternary solvent system (CB : DIO : CN

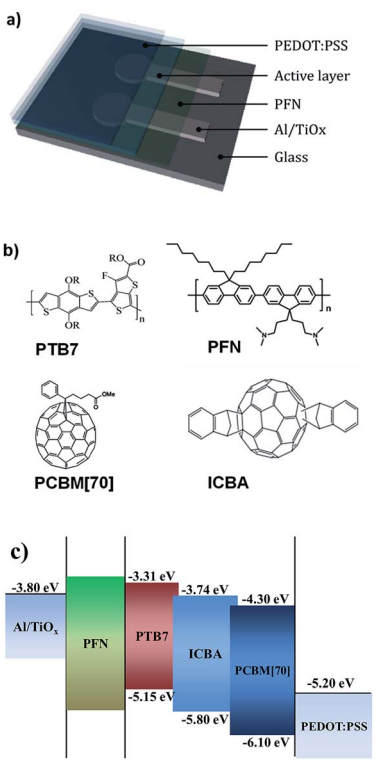

Fig. 1 (a) Schematic of the device structure of the IFISC. (b) Molecular structures of PTB7, PFN, PCBM[70] and ICBA. (c) Schematic energy levels of various materials.

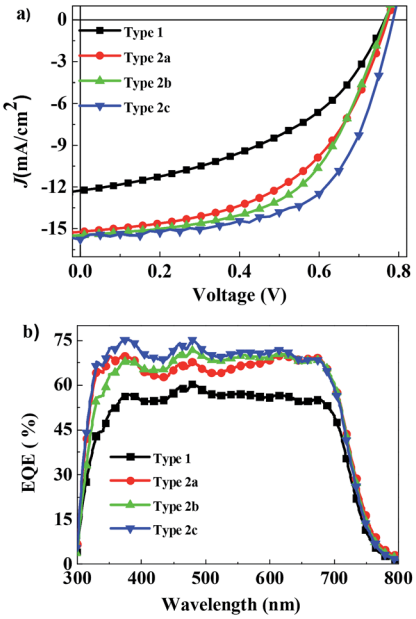

Fig. 2 (a) *J*–*V* and (b) EQE curves of Type 1, Type 2a, Type 2b and Type 2c devices.

94 : 3 : 3 v/v), as shown in Fig. S2 and Table S2,† in which the Type 2c device (10 wt% ICBA) shows an encouraging average PCE of 7.55% with the highest PCE attained being 7.65%. In comparison, the PTB7 : PCBM[70] : ICBA (10 wt% ICBA) ternary solute system device using the binary solvent system CB : DIO (97 : 3 v/v) shows a PCE of only 6.75%. This reveals that the CN solvent and ICBA solute are quite effective at further increasing the IFISC performance. In addition, the PTB7 : ICBA IFISC with the ternary solvent system CB : DIO : CN (94 : 3 : 3 v/v) shows a very low PCE of 3.74%, indicating that the PTB7 : PCBM[70] system can form a finer nanostructure with continuous networks compared to the PTB7 : ICBA system (see Fig. S2 and Table S2†).

To verify the general applicability of the dual ternary system, Type 3 devices with a device structure of ITO/PFN/active layer/MoO_3/Al were fabricated.[3] The ITO-based Type 3c devices with the dual ternary system exhibit an average PCE of 8.33%, which is much higher than the PCE of 7.63% for the Type 3b devices with the binary blend of PTB7 : PCBM[70] processed from the ternary solvent CB : DIO : CN and the PCE of 7.05% from the Type 3a devices with the binary blends of PTB7 : PCBM[70] processed from the binary solvent CB : DIO (see Fig. S3† and Table 1). It is very clear that PCEs increase stepwise when using the dual ternary system for both the ITO-free and ITO-based inverted solar cells. The lower PCE of the Type 2c device than that of the Type 3c device (7.55% *vs.* 8.33%) should be mainly attributed to the lower conductivity of the PEDOT:PSS layer than ITO (760 S cm^{-1} *vs.* 3400 S cm^{-1}). We emphasize that the transmittance spectra of the ITO and PEDOT:PSS films are comparable with the higher transmittance from 300 to 540 nm for PEDOT:PSS and from 540 to 800 nm for ITO, as shown in Fig. S4.† Furthermore, the dual ternary system was also investigated using the conventional device structure ITO/PEDOT:PSS/active layer/Ca/Al, as shown in Fig. S5 and Table S3,† which also demonstrates the same trend in the improvement of the PCE. Thus, we claim that employing the dual ternary system is an effective method for improving the PCE of BHJ solar cells and is a method that is independent of the device architecture.

To confirm the accuracy of the *J*–*V* measurements in Fig. 2a, the corresponding external quantum efficiency (EQE) curves of the IFISCs were plotted as shown in Fig. 2b. All of the devices show broad photoresponses in the wavelength range of 300 nm to 800 nm. The maxima of the EQEs reach 55%, 65%, 70% and 75% for Type 1, Type 2a, Type 2b and Type 2c devices, respectively. The Type 2c device with the dual ternary system shows the highest EQE. The calculated short-circuit currents based on EQE spectra are in good agreement with the measured current values. It was noted that the addition of ICBA into the PTB7 : PCBM[70] active layer has no influence on the profile of the EQE curves of PTB7 : PCBM[70], which is consistent with the ultraviolet-visible (UV-vis) absorption spectra shown in Fig. S6.† This indicates that ICBA makes almost no contribution to the harvesting of photons.

From the *J*–*V* and EQE curves, it can be seen that the use of PFN for the interlayer is necessary as it modifies the Al/TiO_x cathode. Fig. 3 shows the ultraviolet photoelectron spectroscopy (UPS) data for the Al/TiO_x cathodes with and without (w/o) PFN modification. A reduction in the Al/TiO_x cathode work function from −3.8 eV to −3.3 eV, which is determined by the intersection of the curve tangent, is observed after the deposition of the PFN interlayer due to the formation of an interfacial dipole.[3]

Table 1 Device performance measured under AM 1.5G illumination

Type	Active layer[a]	Solvent[b]	Thickness (nm)	J_{sc} (mA cm^{-2})	V_{oc} (V)	FF	Highest PCE (%)	Average PCE (%)
Type 1[c]	PTB7 : PCBM[70] = 1 : 1.5	CB : DIO = 97 : 3	95	12.27	0.76	0.44	4.32	4.12
Type 2a[d]	PTB7 : PCBM[70] = 1 : 1.5	CB : DIO = 97 : 3	95	15.25	0.77	0.51	6.18	6.08
Type 2b[d]	PTB7 : PCBM[70] = 1 : 1.5	CB : DIO : CN = 94 : 3 : 3	90	15.46	0.77	0.56	6.78	6.61
Type 2c[d]	PTB7 : PCBM[70] : ICBA = 1 : 1.5 : 0.25	CB : DIO : CN = 94 : 3 : 3	95	15.80	0.78	0.61	7.65	7.55
Type 3a[e]	PTB7 : PCBM[70] = 1 : 1.5	CB : DIO = 97 : 3	95	15.47	0.77	0.60	7.18	7.05
Type 3b[e]	PTB7 : PCBM[70] = 1 : 1.5	CB : DIO : CN = 94 : 3 : 3	90	16.37	0.77	0.61	7.79	7.63
Type 3c[e]	PTB7 : PCBM[70] : ICBA = 1 : 1.5 : 0.25	CB : DIO : CN = 94 : 3 : 3	95	17.39	0.78	0.62	8.43	8.33

[a] Weight ratio. [b] Volume ratio. [c] With the device structure of Al/TiO_x/active layer/PEDOT:PSS. [d] With the device structure of Al/TiO_x/PFN/active layer/PEDOT:PSS. [e] With the device structure of ITO/PFN/active layer/MoO_3/Al.

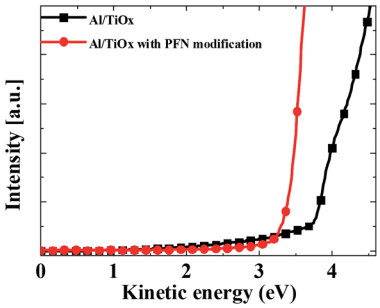

Fig. 3 Normalized UPS spectra of Al/TiO_x cathodes without PFN modification.

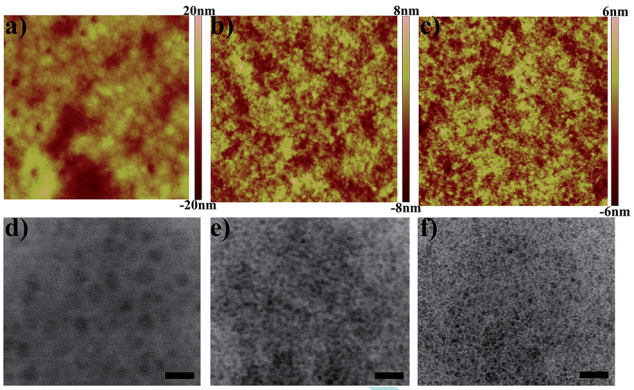

Fig. 4 AFM and corresponding TEM images of active layers of (a and d) Type 2a, (b and e) Type 2b, (c and f) Type 2c devices (AFM image size: 5 μm × 5 μm, TEM bar = 200 nm).

The reduced work function of the Al/TiO_x cathode can increase the built-in potential of the solar cells and offer better energy level alignment with the lowest unoccupied molecular orbital (LUMO) of the organic active layer, which enhances exciton separation and facilitates electron transfer from the active layer to the Al/TiO_x cathode. The results from the UPS data were confirmed by scanning Kelvin probe force microscopy (SKPFM) data, as shown in Fig. S7,† as the work function of the Al/TiO_x decreased after the insertion of the PFN layer.

The surface energy of the Al/TiO_x cathode modified without PFN was investigated by Owen's method, using water and formamide as the control solvents.[34] The contact angle increases from 65° to 85° for water and from 42° to 69° for formamide respectively after spin-coating the PFN layer on top of the Al/TiO_x cathode, leading to a decrease in surface energy from 44.2 mN m^{-1} to 27.0 mN m^{-1} (see details in the ESI†). We emphasize that the difference of the surface roughness of the Al/TiO_x cathode modified with and without PFN is very small (1.19 nm *vs.* 1.89 nm), indicating that surface roughness has little effect on the contact angle. The increase in hydrophobicity due to modification of the Al/TiO_x cathode with PFN is beneficial for the formation of a hole-free and compact PTB7 : PCBM[70] active layer, which can be deposited in orthogonal nonpolar organic solvents.

To further understand the reasons for the different performances of the devices, the morphology of the photoactive films was investigated using atomic force microscopy (AFM). As shown in Fig. 4a–c, the root mean square (RMS) roughness values of the Type 2a, Type 2b and Type 2c active layers deduced from the AFM images are 3.97 nm, 1.87 nm and 1.41 nm, respectively. The addition of CN to the films in the Type 2b devices can promote film uniformity and thus improve the performance of the resulting device, as seen in Fig. 4b. The lowest RMS achieved by the Type 2c film indicates that the BHJ film incorporating the dual ternary system exhibits a smoother surface and probably an improved D : A phase separation, which could be one of the reasons for the higher J_{sc} and FF.

To confirm the observations seen in AFM and get an insight into the domain sizes of the films in the bulk, stereoscopic topographies of the active layers were examined by TEM. In Fig. 4d, the TEM image of the Type 2a pristine active layer displays big domains on the order of about 100–150 nm, where the black domains correspond to PCBM[70] and the white parts correspond to polymer rich domains.[35] When the active layer (PTB7 : PCBM[70]) was processed using the ternary solvent system with 3% CN blended into CB : DIO, much smaller domain sizes were observed as shown in Fig. 4e. Furthermore, when the active layer with 10 wt% ICBA was processed using the ternary solvent system, the domain sizes in the resulting film decreased even further as shown in Fig. 4f. The observations from the TEM images agree well with the images from AFM. A clear correlation between the film morphology and device performance has been observed, whereby films with smaller domain sizes and phase separations give higher performances in devices. This is because the smaller domain sizes are beneficial for the generated excitons to diffuse to the D/A interface and sequentially dissociate into electrons and holes, resulting in reduced germinate charge recombination.[35] The reduced germinate charge recombination and larger D/A interface areas for the dual ternary system should be one of the reasons for their improved performance.

The morphology of the photoactive films is formed during the drying process. This process is greatly influenced by the rate of solvent evaporation. Here, a transient drying monitoring technique was applied to monitor the reflectance images *in situ*, and track the different drying processes that take place in the formation of the Type 2a–c films (seen in Fig. 5).[36,37] The rate of solvent evaporation of the Type 2a film is much greater than that of Type 2b and Type 2c films. The final drying time, determined by the intersection of the curve's tangent and the straight line, is about 400 s for the Type 2a film and 600 s for Type 2b and Type 2c films, respectively. The longer drying time for Type 2b and 2c films can be explained by the higher boiling point of the additive CN (259 °C). Similar solvent evaporation processes that take place in Type 2b and Type 2c films are consistent with their fine AFM morphologies, as shown in Fig. 4.

To further understand the charge transfer (CT) processes in the BHJ active layer of the dual ternary system, highly sensitive electroluminescence (EL) emission and Fourier-transform photocurrent spectroscopy (FTPS) measurements were carried

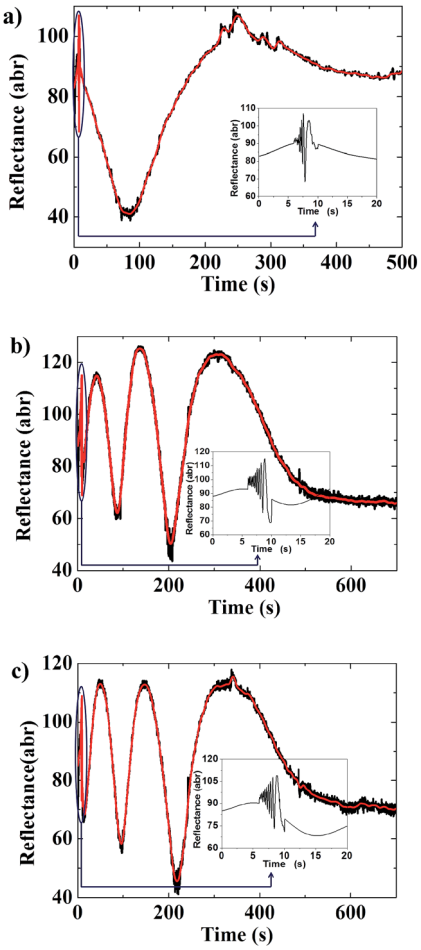

Fig. 5 The drying process of spin-coating (a) Type 2a, (b) Type 2b and (c) Type 2c active layers.

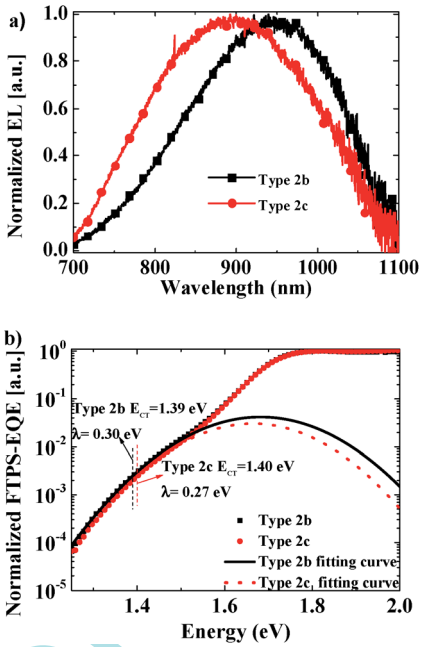

Fig. 6 (a) Normalized EL spectra of Type 2b and Type 2c devices. (b) Normalized FTPS-EQE spectra of Type 2b and Type 2c devices with theoretical FTPS-EQE fitting.

out.[38,39] The EL spectra peaked at 950 nm for Type 2b and 900 nm for Type 2c, as shown in Fig. 6a. These peaks should be attributed to the CT state recombination in D : A BHJ solar cells, as the EL of pure PTB7 has a reported emission peak around 820 nm and pure PCBM[70] has an emission peak at 720 nm.[40,41] The blue-shift in the EL of about nearly 50 nm, after doping with 10 wt% ICBA into the PTB7 : PCBM[70] active layer, indicates that there should be another route to transfer electrons from PTB7 to ICBA besides that from PTB7 to PCBM[70]. The higher LUMO of ICBA means that it can become an intermediate energy level which in turn changes the original charge transfer state of PTB7 to PCBM[70].[29] The theoretical energy of the CT state (E_{CT}) is considered to be the effective band gap of a D : A blend and determines the V_{oc} of a BHJ solar cell. The value of the E_{CT} can be deduced from the measured EQEs of the charge transfer states (EQE_{CT}) using the following equation.[42,43]

$$EQE_{CT}(E) = \frac{f}{E\sqrt{4k\pi\lambda T}} \exp\left(\frac{-(E_{CT} + \lambda - E)^2}{4k\pi\lambda T}\right)$$

where λ is the reorganization energy associated with the charge transfer absorption, T is the temperature, k is the Boltzmann constant and f is the prefactor. From Fig. 6b, we can obtain an E_{CT} of 1.39 eV for Type 2b, and an E_{CT} of 1.40 eV for Type 2c. It has been demonstrated that PCBM[60] and ICBA can form a fullerene alloy so that the V_{oc} of the ternary blend system gradually increases as the content of ICBA increases.[28] However, it is unclear whether this kind of a fullerene alloy can form between PCBM[70] and ICBA, which have different carbon buckyballs. From Fig. 6b, it is clear that the CT state absorption shifts to higher energy upon the addition of 10 wt% ICBA, without producing any new absorption states. This result indicates that PCBM[70] and ICBA can also form an alloy with a LUMO level based on the average composition. Alloy formation implies that the two different fullerene components are subject to intimate and uniform electronic interactions, whereby the delocalization of states is extensive. In addition, the energy shift (~10 meV) corresponds well with the difference in V_{oc} (~10 mV) between the two devices (Type 2b and 2c as well as Type 3b and 3c), indicating that V_{oc} is determined by the polymer and newly formed alloy.[44] The efficient new charge transfer pathway from PTB7 to the fullerene alloy in the ternary system together with the slightly improved V_{oc} should be the partial reason for the improved performance in the dual ternary system compared to the binary system. We emphasize that the ternary solute system has a big effect on the CT emission (~50 nm) and CT state absorption (~10 meV) of the active layers when we compared Type 2a with the PTB7 : PCBM[70] : 10 wt% ICBA device using the same CB : DIO binary solvent system, as shown in Fig. S8a and b,† whereas for Type 2a and Type 2b, the quite same EL (950 nm) and FTPS data (1.39 eV) indicate that the ternary solvent system has little influence on the energy level alignment.

The dual ternary system was checked for the poly(3-hexylthiophene) (P3HT) : PCBM[70] blend system with the ITO-free

inverted device structure of Al/TiO_x/PFN/BHJ/PEDOT:PSS, as shown in Fig. S9 and Table S6.† The ternary solvent system (CB : DIO : CN) device shows a slightly higher PCE compared with the binary solvent system (CB : DIO) (3.04% *vs.* 2.92%). When 10 wt% ICBA was added into the P3HT : PCBM[70] blend to form the dual ternary system (CB : DIO : CN), the average PCE is further improved to 3.56%. In addition, for the conventional device with the structure of ITO/PEDOT:PSS/BHJ/LiF/Al, similar results are obtained, as shown in Fig. S10 and Table S7.† The ternary solvent system (CB : DIO : CN) shows a slightly higher PCE than the binary solvent system (CB : DIO) (2.25% *vs.* 2.16%). For the dual ternary system, the PCE is 2.53%, verifying the general applicability of the dual ternary system.

Conclusions

In this study, it has been demonstrated that very fine nanostructures and matched energy level alignments can be produced using a dual ternary system with CB : DIO : CN as the ternary solvent system and PTB7 : PCBM[70] : ICBA as the ternary solute system for the active layers of PSCs. As a result, device performance was significantly improved in a variety of device architectures including conventional devices (ITO/PEDOT:PSS/active layer/Ca/Al), ITO-based inverted devices (ITO/PFN/active layer/MoO_3/Al) and novel ITO-free inverted devices (Al/TiO_x/PFN/active layer/PEDOT:PSS). To modify the energy level alignment, it is necessary to use an interface layer between the active layer and the bottom TiO_x/Al cathode. It has been found through imaging the surface morphology of the active layer with AFM and TEM and by using optical interference to monitor the transient film formation process that a finer nanostructure can be realized *via* mixing the high-boiling solvent CN into the binary CB : DIO solvent mixture to form a ternary solvent system. Moreover, an improved energy level alignment is obtained by doping ICBA into the binary PTB7 : PCBM[70] blends, whereby the ternary solute system provides a new pathway for charge transfer from PTB7 to the PCBM[70] : ICBA alloy, which is confirmed by EL emission and Fourier transform photocurrent spectroscopy. An encouraging PCE of 7.65% is achieved from the dual ternary system due to the finer morphology and improved energy level alignment, which is the highest value ever reported for an ITO-free inverted polymer solar cell with a spin coated PEDOT:PSS layer as the anode – a system which is completely compatible with low-cost large-area roll-to-roll manufacturing. Moreover, the dual ternary system was also proved to be robust in ITO-based inverted devices, where a PCE of 8.43% was achieved, representing the highest PCE for ternary systems in BHJ solar cells achieved to date.

Experimental section

Materials

PTB7 and P3HT were purchased from 1-Material Inc. and Rieke Metals Inc. PCBM[70] was obtained from Solenne BV. PEDOT:PSS (Clevious PH1000) solution was mixed with 5% dimethyl sulfoxide (DMSO) (Alfa Aesar 99.9%) and 0.5% surfactant (FS-300) for higher conductivity and better surface wettability. PFN and ICBA were synthesized in our lab. All reagents and metals were purchased from Alfa, Dupont, GCRF, and used without further purification.

Device fabrication

The devices were fabricated on glass substrates, which were cleaned in acetone, alkaline lotion, deionized water and isopropanol. Initially, roughly 100 nm of Al and 4 nm of Ti were thermally evaporated onto the glass substrates. Then the bilayer cathode was exposed to air for 12 hours to form the Al/TiO_x cathode. About 5 nm of PFN was spin-coated onto the Al/TiO_x cathode from methanol with a concentration of 0.5 mg mL^{-1} in a glovebox. The PTB7 : PCBM[70] was blended in a ratio of 1 : 1.5 with a concentration of 25 mg mL^{-1} in a binary solvent system of CB : DIO (97 : 3 v/v) or ternary solvent system of CB : DIO : CN (96 : 3 : 1, 94 : 3 : 3, 92 : 3 : 5 v/v). ICBA (5, 10, 15 wt%) was added into the PTB7 : PCBM[70] solution with the ternary solvent (94 : 3 : 3 v/v) to form the dual ternary system. For comparison, a 1 : 1.5 : 0.25 ratio of PTB7 : PCBM[70] : ICBA (10 wt% ICBA) with a binary solvent CB : DIO (97 : 3 v/v) and 1 : 1.5 ratio of PTB7 : ICBA with the ternary solvent CB : DIO : CN (94 : 3 : 3 v/v) were also employed. The BHJ solution was heated at 60 °C overnight to achieve better mixing. The PTB7 : PCBM[70] blend solution was spin-coated on a PFN modified or pure Al/TiO_x cathode to form a 90–100 nm thick active layer. PEDOT:PSS mixed with 5% DMSO and 0.5% surfactant was spin-coated onto the top of the active layer at 1000 rpm and annealed at 60 °C for 30 s to remove any residual water. Finally, the devices were encapsulated with clean glass. The effective device area was 4 mm^2. The fabrication process of the ITO-based inverted and conventional solar cells is similar to that of the IFISCs with MoO_3 (or Ca) and Al deposition thicknesses being 10 nm and 100 nm, respectively. The LiF deposition thickness is 0.7 nm.

TEM sample preparation

About 30 nm PEDOT:PSS (4083) was firstly spin-coated on the ITO glass. Then various active solutions were spin-coated on top of the PEDOT:PSS (4083) layer. The samples were subsequently put into deionized water for few minutes. The floating samples were picked up by copper foil and prepared for TEM observation.

Characterization

The current-density–voltage characteristics were measured using a Keithley 2400 source meter under the illumination of an AM 1.5G solar simulator with an intensity of 100 mW cm^{-2} (Sun 2000 Solar Simulator, Abet Technologies, Inc.). The EQE data were recorded with a QE-200 system from Oriel Company (USA). The UPS data were investigated using an ESCALAB 250 from Thermo-VG Scientific. The SKPFM data were measured using SKP5050 from Cross-Tech. The film thickness was measured with a surface profiler (XP-2). The film topography was investigated using AFM (CSPM5500) and TEM (PHILIPS TECNAI-10). UV-vis absorption spectra were recorded on a Shimadzu UV-

2550 UV-vis spectrophotometer. EL spectra were measured with a Shamrock SR-303i spectrograph from Andor Tech coupled to a Newton EM-CCD Si array detector. The highly sensitive FTPS were obtained using a Vertex 70 from Bruker optics.

Acknowledgements

The authors are grateful to the NSFC Project (#11204106 #61274062 #21225418), the Open Fund of the State Key Laboratory of Luminescent Materials and Devices (South China University of Technology #2012-skllmd-10, #2013-skllmd-06, and #2015-skllmd-02) and the Fundamental Research Funds for the Central Universities for financial support. FG and EW acknowledge the Swedish Research Council (VR) for financial support. EW acknowledges the funding for the author of the Excellent Doctoral Dissertations of Guangdong Province (ybzzxm201114).

Notes and references

1 G. Li, R. Zhu and Y. Yang, *Nat. Photonics*, 2012, **6**, 153.
2 J. You, L. Dou, K. Yoshimura, T. Kato, K. Ohya, T. Moriarty, K. Emery, C.-C. Chen, J. Gao and G. Li, *Nat. Commun.*, 2013, **4**, 1446.
3 Z. He, C. Zhong, S. Su, M. Xu, H. Wu and Y. Cao, *Nat. Photonics*, 2012, **6**, 593.
4 F. C. Krebs, *Sol. Energy Mater. Sol. Cells*, 2009, **93**, 465.
5 F. C. Krebs, *Sol. Energy Mater. Sol. Cells*, 2009, **93**, 1636.
6 Y. Xia, K. Sun and J. Ouyang, *Adv. Mater.*, 2012, **24**, 2436.
7 M. Jørgensen, K. Norrman and F. C. Krebs, *Sol. Energy Mater. Sol. Cells*, 2008, **92**, 686.
8 Z. Tang, L. M. Andersson, Z. George, K. Vandewal, K. Tvingstedt, P. Heriksson, R. Kroon, M. R. Andersson and O. Inganäs, *Adv. Mater.*, 2012, **24**, 554.
9 M. Manceau, D. Angmo, M. Jørgensen and F. C. Krebs, *Org. Electron.*, 2011, **12**, 566.
10 B. A. Collins, J. R. Tumbleston and H. Ade, *J. Phys. Chem. Lett.*, 2011, **2**, 3135.
11 L.-M. Chen, Z. Xu, Z. Hong and Y. Yang, *J. Mater. Chem.*, 2010, **20**, 2575.
12 W. Ma, C. Yang, X. Gong, K. Lee and A. J. Heeger, *Adv. Funct. Mater.*, 2005, **15**, 1617.
13 H. Li, H. Tang, L. Li, W. Xu, X. Zhao and X. Yang, *J. Mater. Chem.*, 2011, **21**, 6563.
14 F. C. Krebs, *Sol. Energy Mater. Sol. Cells*, 2009, **93**, 394.
15 Y. Yao, J. Hou, Z. Xu, G. Li and Y. Yang, *Adv. Funct. Mater.*, 2008, **18**, 1783.
16 J. K. Lee, W. L. Ma, C. J. Brabec, J. Yuen, J. S. Moon, J. Y. Kim, K. Lee, G. C. Bazan and A. J. Heeger, *J. Am. Chem. Soc.*, 2008, **130**, 3619.
17 C. V. Hoven, X. D. Dang, R. C. Coffin, J. Peet, T. Q. Nguyen and G. C. Bazan, *Adv. Mater.*, 2010, **22**, E63.
18 F. Liu, Y. Gu, C. Wang, W. Zhao, D. Chen, A. L. Briseno and T. P. Russell, *Adv. Mater.*, 2012, **24**, 3947.
19 L. Ye, S. Zhang, W. Ma, B. Fan, X. Guo, Y. Huang, H. Ade and J. Hou, *Adv. Mater.*, 2012, **24**, 6335.
20 P. P. Khlyabich, A. E. Rudenko, R. A. Street and B. C. Thompson, *ACS Appl. Mater. Interfaces*, 2014, **6**, 9913.
21 L. Yang, L. Yan and W. You, *J. Phys. Chem. Lett.*, 2013, **4**, 1802.
22 T. Ameri, P. Khoram, J. Min and C. J. Brabec, *Adv. Mater.*, 2013, **25**, 4245.
23 H. Cha, D. S. Chung, S. Y. Bae, M. J. Lee, T. K. An, J. Hwang, K. H. Kim, Y. H. Kim, D. H. Choi and C. E. Park, *Adv. Funct. Mater.*, 2013, **23**, 1556.
24 L. Chen, K. Yao and Y. Chen, *J. Mater. Chem.*, 2012, **22**, 18768.
25 L. Lu, T. Xu, W. Chen, E. S. Landry and L. Yui, *Nat. Photonics*, 2014, **8**, 716.
26 Y. Yang, W. Chen, L. Dou, W. H. Chang, H. S. Duan, B. Bob and G. Li, *Nat. Photonics*, 2015, **9**, 190.
27 P. P. Khlyabich, B. Burkhart and B. C. Thompson, *J. Am. Chem. Soc.*, 2011, **133**, 14534.
28 R. A. Street, D. Davies, P. P. Khlyabich, B. Burkhart and B. C. Thompson, *J. Am. Chem. Soc.*, 2013, **135**, 986.
29 P. Cheng, Y. Li and X. Zhan, *Energy Environ. Sci.*, 2014, **7**, 2005.
30 X. Hu, L. Chen, Y. Zhang, Q. Hu, J. Yang and Y. Chen, *Chem. Mater.*, 2014, **26**, 6293.
31 Z. Tang, W. Tress, Q. Bao, M. J. Jafari, J. Bergqvist, T. Ederth, M. R. Andersson and O. Inganas, *Adv. Energy Mater.*, 2014, **4**, 1400643.
32 T. Yang, M. Wang, C. Duan, X. Hu, L. Huang, J. Peng, F. Huang and X. Gong, *Energy Environ. Sci.*, 2012, **5**, 8208.
33 Z. He, C. Zhong, X. Huang, W. Y. Wong, H. Wu, L. Chen, S. Su and Y. Cao, *Adv. Mater.*, 2011, **23**, 4636.
34 D. K. Owens and R. Wendt, *J. Appl. Polym. Sci.*, 1969, **13**, 1741.
35 F. Liu, W. Zhao, J. R. Tumbleston, C. Wang, Y. Gu, D. Wang, A. L. Briseno, H. Ade and T. P. Russell, *Adv. Energy Mater.*, 2014, **4**, 130137.
36 J. Bergqvist, S. A. Mauger, K. Tvingstedt, H. Arwin and O. Inganäs, *Sol. Energy Mater. Sol. Cells*, 2013, **114**, 89.
37 K. Xiong, L. Hou, M. Wu, Y. Huo, W. Mo, Y. Yuan, S. Sun, W. Xu and E. Wang, *Sol. Energy Mater. Sol. Cells*, 2015, **132**, 252.
38 M. Vanecek and A. Poruba, *Appl. Phys. Lett.*, 2002, **80**, 719.
39 L. Goris, A. Poruba, L. Hod'akova, M. Vaněček, K. Haenen, M. Nesládek, P. Wagner, D. Vanderzande, L. De Schepper and J. Manca, *Appl. Phys. Lett.*, 2006, **88**, 052113.
40 K. Tvingstedt, K. Vandewal, A. Gadisa, F. Zhang, J. Manca and O. Inganas, *J. Am. Chem. Soc.*, 2009, **131**, 11819.
41 W. Zhang, Y. Wu, Q. Bao, F. Gao and J. Fang, *Adv. Energy Mater.*, 2014, **4**, 1400359.
42 K. Vandewal, K. Tvingstedt, A. Gadisa, O. Inganäs and J. V. Manca, *Nat. Mater.*, 2009, **8**, 904.
43 K. Vandewal, K. Tvingstedt, A. Gadisa, O. Inganäs and J. V. Manca, *Phys. Rev. B: Condens. Matter Mater. Phys.*, 2010, **81**, 125204.
44 K. Vandewal, S. Albrecht, E. T. Hoke, K. R. Graham, J. Widmer, J. D. Douglas, M. Schubert, W. R. Mateker, J. T. Bloking and G. F. Burkhard, *Nat. Mater.*, 2014, **13**, 63.